

Space- and time-resolved measurement of rotational wave packet revivals of linear gas molecules using single-shot supercontinuum spectral interferometry

Y.-H. Chen,* S. Varma, and H. M. Milchberg

Institute for Research in Electronics and Applied Physics, University of Maryland, College Park, Maryland 20740, USA

*Corresponding author: yhchen@umd.edu

Received March 19, 2008; accepted March 20, 2008;
posted March 31, 2008 (Doc. ID 94068); published May 28, 2008

Femtosecond laser-induced alignment and its periodic quantum revivals are measured in a range of linear gas molecules using an improved version of single-shot supercontinuum spectral interferometry. In particular, room temperature alignment revivals of hydrogen and deuterium molecules are measured for the first time, to the best of our knowledge, in a single shot. Wave packet collisional dephasing rates are also measured. © 2008 Optical Society of America

OCIS codes: 020.1670, 020.2649, 190.3270, 320.7100, 120.3180, 120.5050.

1. INTRODUCTION

A. Laser Alignment of Linear Molecules and Rotational Wave Packet Revivals

At thermal equilibrium, linear or more complicated gas molecules are randomly oriented and rotate at integer multiples of a fundamental frequency, with populations obeying the Boltzmann distribution. When irradiated by an intense laser pulse ($\sim 10^{13}$ W/cm²), molecules with anisotropic polarizability tend to be aligned such that the most polarizable axis is torqued toward the field polarization axis. After the aligning pulse has passed, the molecules become free rotors again where their rotational states have a common initial phase induced by the pump pulse. After a certain amount of time (a full or a fractional rotation period of the lowest level), the rotational states evolve back to their original phase and their superposition manifests itself as alignment in the absence of the external laser field, or an alignment quantum recurrence. These recurrences are loosely analogous to longitudinal optical modes in a laser cavity that, when given a common phase, can superpose into short bursts of optical energy density (mode-locked pulses) with the repetition duration of a full round trip time in the cavity. Alignment of molecules in intense laser fields, and the subsequent “field-free” realignments, or quantum recurrences, owing to the rephasing of the coherently excited rotational wave packet, have drawn great interest in recent years [1]. Molecular alignment is of interest for studies of high harmonic generation [2–4], field-driven wave packet tomography [5,6], structural studies of molecules [7,8], long-range atmospheric propagation of intense femtosecond laser pulses [9,10], and laser pulse compression [11]. Thus far, all methods for measuring alignment are based on

multishot pump-probe techniques. A popular method, “Coulomb explosion imaging” uses an intense laser pulse (pump) to align the molecules, and an intense ultrashort secondary pulse (probe), scanned through a series of time delays, to strip electrons by field ionization and induce Coulomb explosion. The ion velocities are directed along the molecular axis, angularly resolved with respect to the pump polarization, giving the time-resolved alignment of an ensemble of molecules [12,13]. The earliest purely optical measurements of alignment were applied to picosecond optical Kerr gating in liquids [14,15]. A linearly polarized pump pulse torqued CS₂ molecules into alignment, inducing a transient birefringence sampled by the polarization rotation imposed on a variably delayed probe pulse. It was later realized that probe pulse delays long after the pump could sample “rotational recurrences” of the molecular alignment if this measurement were performed in much less collisional CS₂ vapor [16]. This technique, now called optical Kerr effect (OKE) spectroscopy [17], has been used to measure a wide range of molecular alignment dynamics. Other optical methods use probe beam refraction from aligned molecular gas samples [18] and ionization of these samples [19]. Spectral modulations imposed on sequentially delayed short probe pulses have also been used to map out wave packet recurrences, although the time resolution of these measurements is limited by the relatively long (>50 fs) probe pulse duration, and quantitative molecular response is obtained only through complex propagation model-dependent fits to the shifted spectra [20,21].

To date, the only technique capable of direct quantitative measurement of alignment is Coulomb explosion imaging [12,13]. However, this method does not provide spa-

tial resolution, and it requires time-consuming multishot scanning. We present here, for the first time to the best of our knowledge, single-shot *quantitative* measurements of the temporal evolution of molecular alignment, with 1D spatial resolution across the laser beam, using single-shot supercontinuum spectral interferometry (SSSI).

B. Single-Shot Supercontinuum Spectral Interferometry SSSI, first developed by Kim *et al.* [22], is a variation of spectral (or frequency domain) interferometry (SI) [23]. SI is a sensitive technique to detect tiny and ultrafast transient refractive index shifts in a medium, which are usually induced by short-duration and intense laser fields via several different mechanisms, including, for example, the optical Kerr ($\chi^{(3)}$) effect [24,25], femtosecond laser-produced plasma evolution [26,27], plasma shock wave dynamics [28], and plasma wakefields [29–31]. With its advantages of high sensitivity and simplicity, SI has become a standard experimental methodology in ultrafast optics and high field physics.

However, the major flaw of standard SI is that it is a multishot method based on a step-by-step scanning through the desired range of time delays, which is susceptible to both shot-to-shot fluctuations and long-term drift. Furthermore, the ultimate time resolution is limited by the shortest pulse duration available from the laser system. In the SI apparatus, two short, weak and identical laser pulses (“reference” and “probe”) with temporal separation τ propagate collinearly along with an intense pump pulse through the interaction zone, and spectrally interfere in the spectrometer. The probe overlaps with the transient pump-induced refractive index change of the medium so that it gains a phase shift, while the reference arrives earlier and is not affected. The recorded interferogram consists of a frequency dependent series of fringes with frequency spacing $2\pi/\tau$ plus a shift caused by the pump-induced perturbation of the refractive index. This phase shift can be directly extracted from the interferogram. The full evolution of the transient refractive index is retrieved by stepping through relative time delays between the pump pulse and the reference–probe pulse pair, assuming that the probe pulse duration is much shorter than the time scale of refractive index modulation.

The demand is therefore that the laser system have extremely stable shot-to-shot reproducibility, since the transient phase shift induced in the probe pulse depends nonlinearly on the pump pulse envelope. Otherwise, the measured refractive index variation between two specific time delays could be caused by laser system pulse-to-pulse fluctuations, potentially burying the real signal. In practice, even with the best efforts, fluctuations cannot be fully eliminated from ultrafast high power laser systems, and thus it is usually necessary to do multishot averaging for each probe delay, a time-consuming task. Moreover, during the long time for a complete delay scan, drifts of laser output energy, spectrum, and pulse shape are usually unavoidable, and these can contribute systematic errors.

The best solution to these difficulties is to utilize a *single-shot* measurement scheme. In SSSI, the short-duration probe and reference pulses are replaced by a

pair of broadband (~ 100 nm) and highly chirped pulses, which are generated from supercontinuum (SC) generation and then temporally stretched by appropriate lengths of dispersive materials in the SC beam path. The probe pulse now fully overlaps the whole event of the transient refractive index evolution, in contrast to only a small partial coverage in the case of standard SI. The nearly linearly chirped probe pulse has a time-dependent frequency sweep $\omega = \omega_0 + bt$, where $b \approx 1/2\beta_2^{-1}[1 + 2\beta_2^{-2}(\Delta\omega)^{-4}]^{-1}$ is the chirp parameter, $\beta_2 = 1/2[\partial^2\phi(\omega)/\partial\omega^2]_{\omega_0}$ is the group delay dispersion at center frequency ω_0 , and $\Delta\omega$ is the bandwidth. The pump-induced time-dependent phase shift is thus encoded onto different frequency components on each time slice of the probe pulse, in a single shot. One may thus be tempted to retrieve the temporal phase evolution by “frequency-to-time mapping” of extracted spectral phase from the interferogram. However, it has been shown that in this approach the temporal resolution is degraded from transform-limited resolution $\Delta t_{\text{res}} \sim (\Delta\omega)^{-1}$ to $\Delta t_{\text{res}} \approx (\Delta\omega)^{-1}[1 + 2\beta_2^2(\Delta\omega)^4]^{1/2}$ [22]. To record longer duration events, one must stretch the probe pulse longer, that is, increase β_2 , which makes time resolution even worse.

In SSSI, to take advantage of a potentially large $\Delta\omega$ and achieve the best time resolution, the full knowledge of spectral amplitudes of probe and reference $|\tilde{E}_{pr}(\omega)| \propto [I_{pr}(\omega)]^{1/2}$, $|\tilde{E}_r(\omega)| \propto [I_r(\omega)]^{1/2}$, along with the spectral phase difference $\Delta\phi(\omega) = \phi_{pr}(\omega) - \phi_r(\omega)$ extracted from the interferogram, are used to obtain the *exact* probe temporal phase shift $\Delta\Phi(t)$ by Fourier transform. If an imaging spectrometer is used, the phase shift can be spatially resolved along the direction of the entrance slit, and a temporally and 1D spatially resolved phase shift $\Delta\Phi(x, t)$ can be used to determine the transient refractive index $n(x, t)$ from $kn(x, t)L = \Delta\Phi(x, t)$, where k is the probe vacuum wavenumber, x is the spatial coordinate transverse to the probe beam, and L is the effective interaction length in the medium.

To meet the requirement of a broadband probe pulse, SC generation in a gas was used as a cheap and convenient solution. Initially that gas was room air. A total SC energy of the order of 10 to 100 μJ with ~ 100 nm bandwidth and central wavelength ~ 690 nm was generated by focusing a 70 fs, 1 mJ, 800 nm Ti:sapphire laser pulse in atmospheric air [22], which resulted in a temporal resolution of ~ 10 fs [32]. Note that at this probe wavelength, the pump-probe walk-off during propagation through the interaction region is negligible. For SI schemes using second-harmonic probe pulses [33], pump-probe walk-off can be a problem. The versatility of SSSI has allowed successful study of many phenomena: transient Kerr nonlinearity in a solid [22], laser-induced double step ionization of He [32], laser-heated cluster explosion [34–36], and intense laser coupling into plasma waveguides [37]. Recently, another version of single-shot interferometry with a broadband chirped probe pulse from the second-harmonic generation of the pump pulse wavelength was used to measure laser wakefields [38], but with less temporal resolution and more walk-off than with SSSI.

The paper is organized as follows. First, we report an improved SSSI setup employing a commercial kilohertz

regenerative amplifier (RGA) system and a sealed Xe gas cell for SC generation at much lower laser energy. We discuss in detail this new configuration and, as proof of principle, report results for the transient Kerr nonlinearity in Ar gas. Second, using the density matrix formalism and first-order perturbation theory, we discuss the effect of alignment of linear molecules on the transient refractive index, through an ensemble averaged quantity $\langle \cos^2 \theta \rangle$, where θ is the angle between the laser field polarization and the molecular axis. Third, we present single-shot measurements of field alignment of molecules near the laser pulse and the field-free alignment recurrences that appear long after the laser pulse has passed, by retrieving the transient phase shift applied to the probe pulse by the pump-induced, ensemble-averaged molecular dynamics in the gas. Note that in the presence of the laser field, the molecular response has two components: a nearly instantaneous bound electron response that contributes to the nonlinear refractive index n_2 , and a slower component that corresponds to the rotation of the molecular axis toward the laser polarization direction. The molecules experience the torque given by the laser field strength and the molecular polarizability, and the moment of inertia determines the rotation time scale.

2. EXPERIMENTAL SETUP

In this work, a 110 fs Ti:sapphire RGA with 1 kHz repetition rate is used. As shown in Fig. 1, the laser output is split into two arms by a beam splitter (BS1). To generate SC, one of the pulses split from BS1 with $\sim 300 \mu\text{J}$ energy is focused into a Xe-filled gas cell (XGC), with pressure adjustable from 0 to 2 atm. The transversely spatially chirped conical emission from the filament, with approximately $30 \mu\text{J}$ per pulse, is collected by a lens and converted into a weakly converging beam. Then a Michelson interferometer (MI) is used to generate twin copropagating SC reference and probe pulses with variable relative

time delay. A $500 \mu\text{m}$ diameter pinhole (P) after the interferometer filters the converging beam spot to shape the beam profile and reduce the spatial chirp with little energy loss. The SC beam is then collimated by a telescope, and a dispersive 2.5 cm thick SF4 glass window is used to stretch the reference and probe pulses to ~ 2 ps, providing a ~ 2 ps temporal window for single-shot transient refractive index measurements.

The laser pulse from the other output of BS1, with tunable delay with respect to SC reference and probe pulses, acts as pump, and a half-wave-plate (HWP) rotates its polarization. Another beam splitter (BS2) recombines the SC probe–reference and pump beam paths, and these three collinearly propagating pulses are focused by an $f = 41$ cm lens into a 45 cm long high pressure gas cell. The pump beam focal spot full width at half-maximum (FWHM) is $36 \mu\text{m}$ by $27 \mu\text{m}$, with a Rayleigh range $z_0 = 4.5$ mm in the cell. The probe beam size is much smaller than the pump before the focusing lens, and therefore overfills the pump at the interaction region near the focus, with a FWHM focal spot size of $270 \mu\text{m}$ and a corresponding Rayleigh range of 24.6 cm. This allows spatially resolved phase shift measurements across the full pump beam profile. The SC reference and probe at the pump interaction region are imaged onto the spectrometer slit with $6.9\times$ magnification. The imaging spectrometer, with a 10-bit CCD camera in the focal plane, provides a ~ 72 nm spectral window ranging from 652 to 723 nm with 1D spatial resolution of $0.67 \mu\text{m}/\text{pixel}$ at the interaction region along the entrance slit direction. We label this direction as the x axis throughout this paper.

The probe temporal phase shift $\Delta\Phi(x, t)$ can be obtained through a Fourier transform if the full spectral phase $\phi_{pr}(\omega) = \phi_r(\omega) + \Delta\phi(\omega)$ of the probe pulse is known. $\Delta\phi(\omega)$ can be directly extracted from the interferogram, and the reference pulse phase $\phi_r(\omega)$ is obtained from the second-order dispersion with the approximation $\phi_r(\omega) \approx \beta_2(\omega - \omega_0)^2$. β_2 is obtained by a series of cross-phase modulation measurements in Ar, varying the pump-probe delay. This is similar to the method described in [22], where a thin glass window was used as the nonlinear medium. The peak frequencies of modulated spectral phase $\Delta\phi(\omega)$ are recorded with respect to their corresponding time delays, and a linear fit of this time versus frequency plot gives the linear chirp parameter $1/b = a = 2\beta_2[1 + (2 \ln 2)^2 \beta_2^{-2} (\Delta\omega)^{-4}] = 7820 \text{ fs}^2$, agreeing well with the calculated total dispersion introduced by materials in the beam path. The higher-order dispersion terms are negligible for the transient phase modulation time scales of interest [22], and for our SC probe bandwidth of ~ 100 nm, we have $\beta_2^{-2} (\Delta\omega)^{-4} \ll 1$ and therefore $\beta_2 \approx a/2$.

In our previous work [22,32,34–37] SC was generated by focusing in 1 atm air a ~ 1 mJ, 70 fs laser pulse split from a 10 Hz, 2 TW Ti:sapphire laser system. In the experiments of this paper, using a lower energy kilohertz laser, the pulse energy is insufficient for SC generation in air with adequate energy and bandwidth. We therefore chose Xe as the SC generation medium because of its large nonlinearity; Xe has been previously observed to generate very broad SC spectra under femtosecond laser pulse illumination [39]. A bonus of using the kilohertz RGA is that we obtain extremely stable SC on a shot-to-

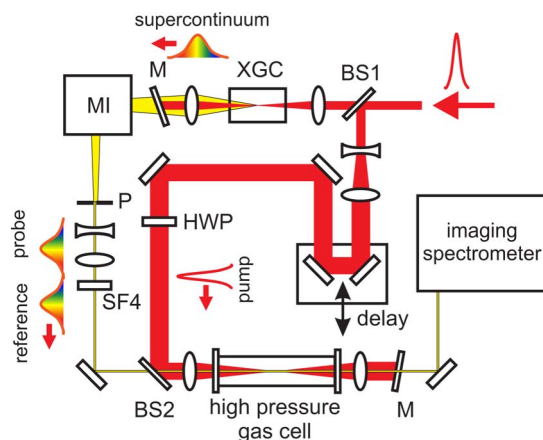


Fig. 1. (Color online) Improved SSSI experimental setup, employing a xenon gas cell to generate broadband supercontinuum. BS1: beam splitter; XGC: xenon gas cell; MI: Michelson interferometer; P: $500 \mu\text{m}$ pinhole; SF4: 2.5 cm thick SF4 glass; HWP: half-wave-plate; M: zero degree dielectric mirror to reject Ti:sapphire laser energy; BS2: beam splitter for combining pump and SC pulses. The pump beam energy can be tuned by another set of half-wave-plate and polarizer, which is not shown in the figure.

shot basis. In general, kilohertz RGAs are far more stable than higher energy 10 Hz systems: the high energy amplifiers of 10 Hz multistage Ti:sapphire laser systems are usually pumped by flashlamp-pumped, Q -switched, frequency-doubled Nd:YAG lasers with pulse-to-pulse energy fluctuation of 10%–15%, while kilohertz RGAs are pumped by Q -switched lasers pumped by CW arc lamps (our system) or high power diodes. Typical kilohertz RGA pulse energy fluctuation is less than 2%.

3. TRANSIENT NONLINEAR REFRACTIVE INDEX IN Ar

A sample spectral interferogram and the corresponding extracted transient refractive index shift $\Delta n(x, t)$ using Ar gas at room temperature are shown in Figs. 2(a) and 2(b), respectively. Ar is a monatomic gas, and its lowest-order nonvanishing nonlinearity near 700–800 nm is the electronic response $\chi^{(3)}$, which is nearly instantaneous, non-resonant, and dispersionless. Below the ionization threshold ($\sim 10^{14}$ W/cm² [40,41]), the nonlinear phase shift imposed on a probe pulse propagating along z is $\Delta\Phi_{\text{Ar}}(x, t) = k \int \Delta n(x, z, t) dz = kn_{2,\text{Ar}} \int I(x, z, t) dz$, where $n_{2,\text{Ar}}$ is the nonlinear refractive index of Ar. An effective nonlinear interaction length L is defined by writing $\Delta\Phi_{\text{Ar}}(x, t) = k\Delta n(x, t)L = kn_{2,\text{Ar}}I(x, t)L$. The nonlinear phase shift follows the time and 1D transverse pump intensity profile $I(x, t)$.

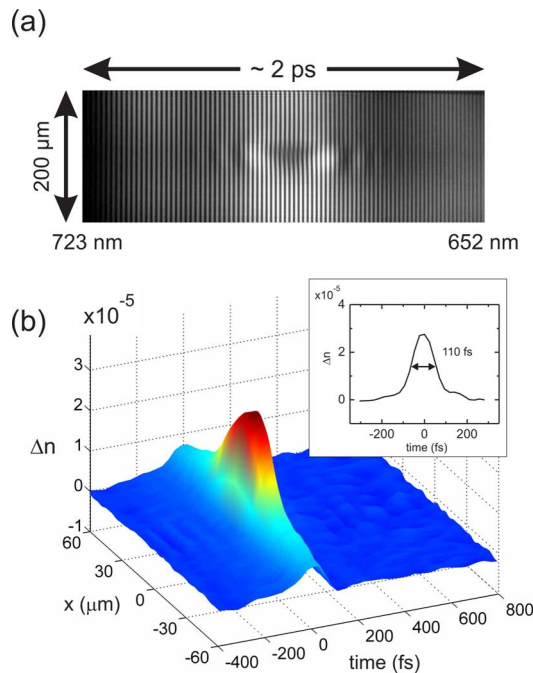


Fig. 2. (Color online) (a) Spectral interferogram showing pump-induced, wavelength-dependent fringe shift, and (b) extracted 1D space and time variations of the effective transient refractive index shift Δn in argon at 7.8 atm pressure and 4.1×10^{13} W/cm² peak pump intensity. The inset in (b) shows the 1D lineout of Δn along $x=0$ axis with a FWHM of ~ 110 fs, which is close to the pump laser pulse duration measured by FROG. The index shift is due to instantaneous electronic nonlinearity and thus follows the pump pulse temporal profile.

Unlike the case of a thin gas jet with a well-defined thickness $\ll 2z_0$, so that the interaction length L is well-defined [32], a gas cell with length $> 2z_0$ requires more careful consideration. Here, we use the extracted nonlinear phase shift from the Ar gas cell experiment to define an effective nonlinear interaction length L , and apply this effective length to all measurements of other species of gases in the same cell, assuming the pump beam profile and convergence is always the same. The procedure is to compare the measured nonlinear phase shift in the Ar gas cell to that in a thin ($\ll 2z_0$) BK7 window with known thickness (200 μm in our case). We obtain the effective length $L = (\Delta\Phi_{\text{Ar}} n_{2,\text{BK7}}) / (\Delta\Phi_{\text{BK7}} n_{2,\text{Ar}}) L_{\text{BK7}} = 5.7$ mm, using values of $n_{2,\text{BK7}} = 3 \times 10^{-16}$ cm²/W measured by SSSI [42] and $n_{2,\text{Ar}} = 9.8 \times 10^{-20}$ cm² W⁻¹ atm⁻¹ from [43]. This effective length is used to determine the refractive index shift throughout this paper. Also note that the measured $n_{2,\text{BK7}}$ value is in good agreement with various values (3.43×10^{-16} , 3.63×10^{-16} , 3×10^{-16} cm²/W) given by, respectively, [44–46].

The 2 ps measurement window of SSSI can be moved with an optical delay line to times well past the pump pulse. In this manner, we can also measure, in a single shot, the refractive index effect of the quantum rotational recurrences induced by pump pulses in molecular gases.

4. TRANSIENT REFRACTIVE INDEX DRIVEN BY FIELD-INDUCED ALIGNMENT OF LINEAR MOLECULES

For an ensemble of linear molecules, the average molecule orientation affects the index of refraction because the molecular polarizability is anisotropic. In the ensemble, if molecular alignment is induced by a pump laser field, the refractive index shift experienced by a probe pulse polarized parallel to the pump is given by

$$\Delta n(t) = 2\pi N n_0^{-1} \Delta\alpha \left(\langle \cos^2 \theta \rangle_t - \frac{1}{3} \right), \quad (1)$$

where N is the number of molecules per unit volume, $\Delta\alpha = \alpha_{\parallel} - \alpha_{\perp}$ is the difference of polarizability parallel and perpendicular to the molecular axis (the longer, more polarizable axis of the linear molecule), θ is the angle between the laser field and the molecular axis, and $\langle \rangle_t$ denotes a time-dependent ensemble average over the molecules. The degree of alignment of a particular molecule is defined to be $\cos^2 \theta$, and its time-dependent ensemble average is calculated as $\langle \cos^2 \theta \rangle_t = \text{Tr}[\rho(t) \otimes \cos^2 \theta] = \rho_{kl}(l|\cos^2 \theta|k)$, where $\rho(t)$ is the density matrix, and where $|l\rangle$ and $|k\rangle$ are molecular rotational eigenstates of the field-free Hamiltonian. For an unperturbed ensemble, the molecules are randomly oriented, with $\langle \cos^2 \theta \rangle_{t=-\infty} = 1/3$. The density matrix is calculated to first order in the optical perturbation, $\rho(t) = \rho^{(0)} + \rho^{(1)}(t)$, and the perturbed density matrix element is

$$[\rho^{(1)}(t)]_{kl} = -\frac{i}{\hbar} \int_{-\infty}^t d\tau [\tilde{h}(\tau), \rho^{(0)}]_{kl} e^{i(\omega_{kl} + \gamma_{kl})(\tau-t)}, \quad (2)$$

where $\tilde{h} = -1/2 \mathbf{p} \cdot \mathbf{E}$ is the perturbation Hamiltonian, $[\]$ denotes a commutator, $\omega_{kl} = (E_k - E_l)/\hbar$ corresponds to ro-

tational states $|k\rangle=|j,m\rangle$ and $|l\rangle=|j',m'\rangle$ with energies $E_k=E_{j,m}=\hbar c B j(j+1)$, $B=\hbar(8\pi^2 c I)^{-1}$ is the rotational constant, I is the molecular moment of inertia, and γ_{kl} is the dephasing rate between states k and l . For a laser field $\mathbf{E}(t)=\hat{\mathbf{e}}\varepsilon(t)\cos\omega t$, where $\varepsilon(t)$ is a slowly varying envelope, we get [47]

$$\langle \cos^2 \theta \rangle_t = \frac{1}{3} - \frac{1}{15\hbar} \Delta\alpha \sum_j \left[\frac{j(j-1)}{2j-1} (\rho_j^{(0)} - \rho_{j-2}^{(0)}) \times \text{Im} \left(e^{i(\omega_{j,j-2} - \gamma_{j,j-2})t} \int_{-\infty}^t d\tau \varepsilon^2(\tau) e^{(-i\omega_{j,j-2} + \gamma_{j,j-2})\tau} \right) \right], \quad (3)$$

where $\omega_{j,j-2}=(E_j-E_{j-2})/\hbar=4\pi c B(2j-1)$.

Note that in our experimental setup, the pump and probe polarizations can also be perpendicular. In that case, the refractive index shift experienced by the probe is

$$\Delta n(t) = 2\pi N n_0^{-1} \Delta\alpha \left(\frac{1}{2} \langle \sin^2 \theta \rangle_t - \frac{1}{3} \right), \quad (4)$$

which gives a result similar to Eq. (1) with half of the magnitude of the transient term, and its sign is flipped.

5. RECURRENCES OF THE COHERENTLY EXCITED ROTATIONAL WAVE PACKET

As discussed, many rotational levels (frequencies) are excited by the aligning pulse. Thus, for most times the ensemble average of the alignment resembles the random thermal average (1/3). However, at special times, the ensemble average of the molecular rotors displays sharp bursts of alignment. To better understand this effect, we express the rotational wave packet of the molecules as the superposition of rotational states $|\psi\rangle=\sum_{j,m} a_{j,m} |j,m\rangle \times \exp(-i\omega_j t)$, where $\omega_j=E_j/\hbar=2\pi c B j(j+1)$. The femtosecond aligning pulse gives a quasi-impulsive torque to initially align the molecules, which equivalently fixes the relative phases among the states. As $|\psi\rangle$ evolves in time each $|j,m\rangle$ state advances with its own phase factor $\exp(-i\omega_j t)$, so that a sum over a large number of states tends to result in cancellation. However, when time passes through $t=qT$, where q is an integer and $T=(2cB)^{-1}$, we have $\omega_j t=q\pi j(j+1)$, and the phases become integer multiples of 2π , causing a ‘‘full revival’’: all states return to their initial condition in the presence of the aligning pulse (neglecting collisions). There also exist ‘‘partial revivals’’ at specific fractions of T . When $t=q(T/2)$ and q is odd (‘‘half-revival’’), $\omega_j t=q\pi j(j+1)/2$. This puts even and odd j states separately in phase, with a phase difference of π . These two sets of j states interfere with each other, leading to a different refractive index response from the full revival case. Partial revivals can also occur at times $T/4$, $T/8$, $T/16$, etc., because $j(j+1)$ is even. Fractional revivals at shorter intervals than quarter revivals are difficult to observe, because they contain more subsets of in-phase states possessing different relative phases. These subsets tend to cancel each other and thus the wave packet amplitude is much weaker. The peak amplitude of partial revivals also depends on nuclear spin statistics [48].

6. EXPERIMENT

A. Rotational Inertia Effect: Delayed Initial Alignment by the Laser Field

The calculated (solid curve) and measured (open circles) transient refractive index shifts in N_2 and N_2O near the 110 fs pump pulse are shown in Figs. 3(a) and 3(b). To compare the effect of rotational inertia, the peak magnitudes of Δn for both gases are normalized to 1. The rotational constants used in the calculation are $B_{N_2}=2.0\text{ cm}^{-1}$ in Fig. 3(a) for N_2 , $B_{N_2O}=0.41\text{ cm}^{-1}$ in Fig. 3(b) for N_2O [49]. The laser field gives an initial ‘‘kick’’ to the molecules, and due to rotational inertia they do not line up along the laser field instantaneously. Thus in Figs. 3(a) and 3(b), Δn peaks later than the driving laser pulse, with the peak for N_2 leading that of N_2O . This is understood from the larger N_2O moment of inertia I , where $B=\hbar(8\pi^2 c I)^{-1}$. Moreover, as the coherently excited rotational wave packet of N_2O evolves more slowly than that of N_2 , its Δn falls back to zero more slowly than the Δn for N_2 . Note that in the calculation of Fig. 3, the instantaneous electronic nonlinear response ($\chi^{(3)}$) is not included, but the measurements still agree well with the calculations. This implies that the alignment effect of the N_2O and N_2 molecules dominates the isotropic prompt electronic response $n_2 I$. This differs from [10], where the prompt response and the rotational inertia effects for N_2 are considered to contribute approximately equally to the transient refractive index. This issue is important for studies of long-range propagation and filamentation of femtosecond laser pulses in the atmosphere [9,10,20,50]. Figure 3(c) compares unnormalized Δn results using 4.4 atm Ar, N_2 , and N_2O , with 95 μJ pump energy ($6.7 \times 10^{13}\text{ W/cm}^2$ peak intensity) for Ar, 60 μJ ($4.2 \times 10^{13}\text{ W/cm}^2$ peak intensity) for N_2 , and 20 μJ ($1.4 \times 10^{13}\text{ W/cm}^2$ peak intensity) for N_2O .

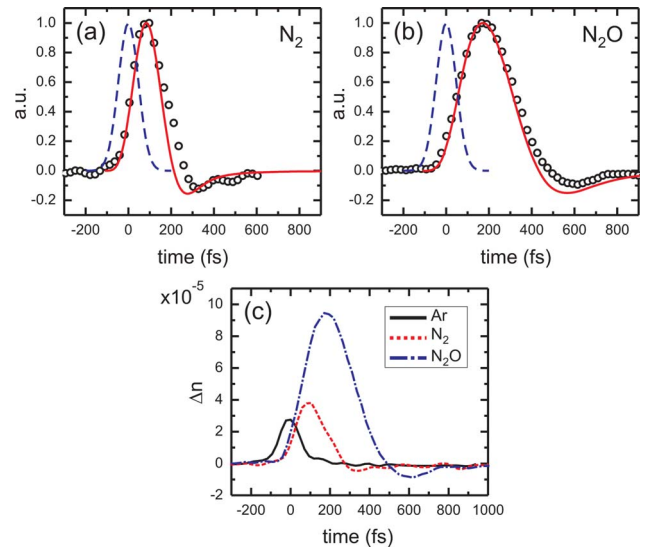


Fig. 3. (Color online) Normalized transient shift of refractive index Δn from measurements (open circles) and calculations (solid curve) for (a) N_2 and (b) N_2O . For comparison, a Gaussian function centered at $t=0$ with 110 fs FWHM duration is shown on each figure (dashed curve) to represent the pump pulse envelope. Unnormalized Δn traces of (a) and (b), along with Ar, are shown in (c), under the experiment conditions of 110 fs pump pulse duration and 4.4 atm Ar, N_2 , and N_2O , with 95 μJ ($6.7 \times 10^{13}\text{ W/cm}^2$), 60 μJ ($4.2 \times 10^{13}\text{ W/cm}^2$), and 20 μJ ($1.4 \times 10^{13}\text{ W/cm}^2$) pulse energy (peak intensity), respectively.

$\times 10^{13}$ W/cm² peak intensity) for N₂, and 20 μ J (1.4 $\times 10^{13}$ W/cm² peak intensity) for N₂O. The Ar response is the purely prompt nonlinear electronic response. N₂ and N₂O measurements were conducted at lower energies than Ar, however they still introduce larger index shifts, again implying that the orientational effect dominates in N₂ and N₂O. Note that as seen later in this paper, for H₂ and D₂ the prompt n_2I response is larger than the alignment response under our experiment conditions.

B. Refractive Index Quantum Echoes Due to Rephasing of the Rotational Wave Packet

To demonstrate SSSI's capability of spatially resolved measurement, Fig. 4 shows an $x-t$ perspective plot of the measured full revival of O₂ alignment $\langle \cos^2 \theta \rangle_t - 1/3$. The time window is centered at $T = (2cB_{O_2})^{-1} = 11.6$ ps [49], and the pump pulse energy is 40 μ J, with 110 fs duration and peak intensity 2.7×10^{13} W/cm². The complete laser-alignment and successive wave packet revivals from $t=0$ through $t=1.25T$ are shown in Fig. 5(a), which are lineouts at the center of the pump beam focus. The results are compared with the calculations shown in Fig. 5(b), using $B_{O_2} = 1.44$ cm⁻¹ and $\Delta\alpha_{O_2} = 1.14 \times 10^{-24}$ cm³ [49]. In Fig. 5(b), two different cases are considered: a delta function pulse with fluence matching the experiment, and a 110 fs duration pulse with a cosine-squared envelope. A damping rate of $\gamma_{j,j-2} = \gamma = 4.31 \times 10^{10}$ s⁻¹ (or dephasing time $1/\gamma = 23.2$ ps) was used in the calculation. This damping rate is obtained from the experiment, by fitting the peak revival amplitudes versus time in Fig. 5(a). We neglect the j dependence of the dephasing rate, as the dephasing is dominated by elastic molecular collisions.

In our calculation shown in Fig. 5(b), results using the delta function pump pulse show good agreement with the experiment (which uses a 110 fs pump pulse). This is because the composition of the rotational wave packet is limited by the temperature. Hence in our case, increasing the pump laser bandwidth to infinity (for the delta function) does not help excite significant additional rotational states at higher energy. Due to the thermal distribution of rotational states before the pump arrives, the most populous state in the excited wave packet is $j = j_{\max} \sim 3/4\{1$

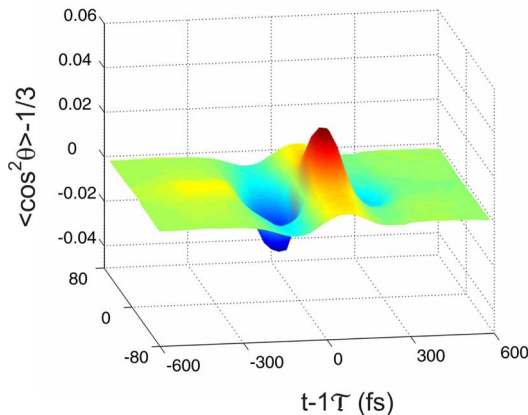


Fig. 4. (Color online) Time-resolved and 1D space-resolved plot of measured full revival of O₂ alignment $\langle \cos^2 \theta \rangle_t - 1/3$, with 5.1 atm gas pressure and 40 μ J pump pulse energy (2.7×10^{13} W/cm² peak intensity).

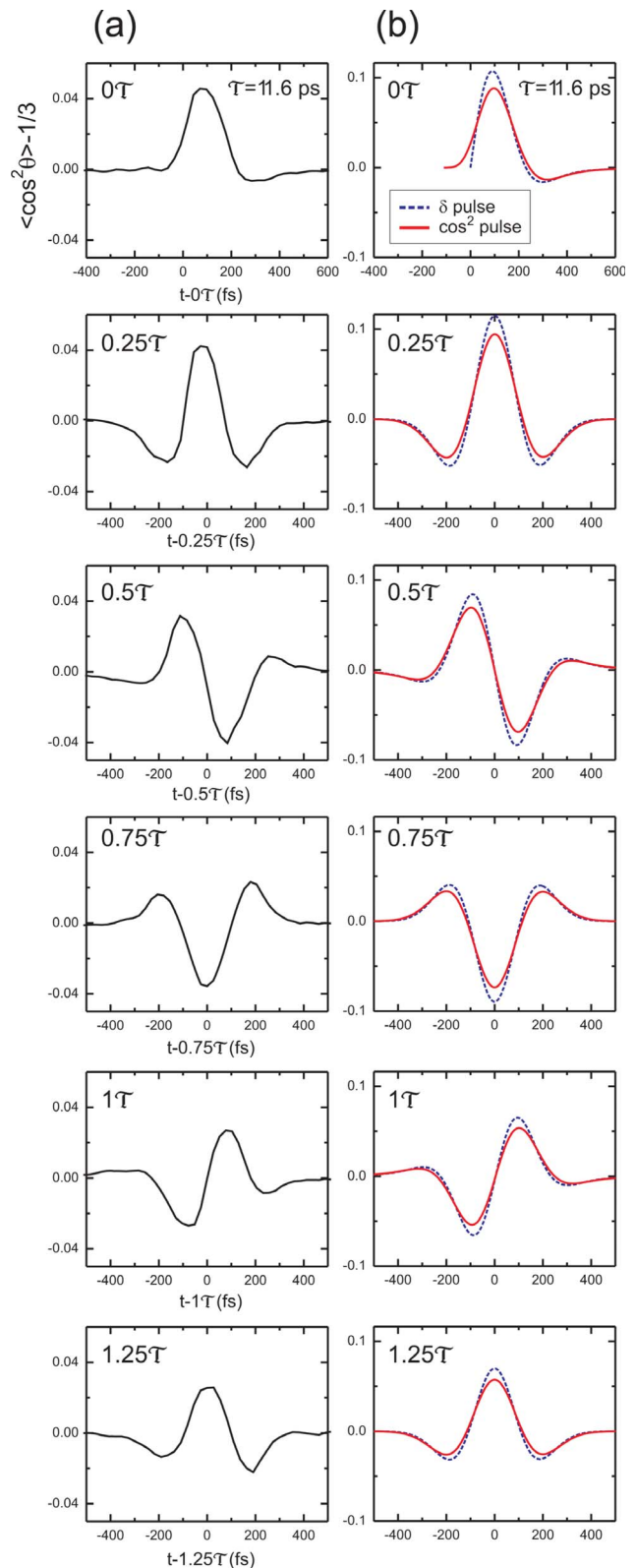


Fig. 5. (Color online) (a) Measured and (b) simulated laser alignment of O₂ molecules and the successive wave packet revivals from $t=0$ to $t=1.25T$, at the center of the pump beam focus ($x=0$), under the same conditions as in Fig. 4. The dephasing time constant $1/\gamma = 23.2$ ps is determined by fitting the peak amplitudes at each revival in (a), and the fitted γ is used to calculate (b). δ function (dashed curve) and \cos^2 function with 110 fs FWHM duration (solid curve) of pump pulse profiles are considered in (b).

$+ [1 + 8/9(k_B T/Bhc)]^{1/2}$. For the case of O_2 molecules at room temperature, we have $k_B T/Bhc \gg 1$ and therefore $j_{\max} \sim (k_B T/Bhc)^{1/2} \sim 13$. It also can be shown that the frequency width of the thermal distribution of rotational states is approximately $\Delta\omega_{\text{rot}} \sim k_B T/\hbar \sim 4 \times 10^{13} \text{ s}^{-1}$ for large j_{\max} . Our pump laser bandwidth $\sim 3 \times 10^{13} \text{ s}^{-1}$ is comparable with $\Delta\omega_{\text{rot}}$, which means the pump laser frequency components already overlap the thermal distribution, and further increasing the laser bandwidth has little effect.

D_2 and H_2 molecules have the smallest moments of inertia and largest rotational constants B (and therefore rotate the fastest). As well, their polarizability asymmetry $\Delta\alpha$ is smaller than for the other molecules of this paper. It is therefore much more difficult to excite and measure the wave packet revivals. To extract the much smaller expected phase shifts we adopted a new method for interferogram analysis. Dark current and readout noise from the CCD sensor chip are the major noise sources masking the measurement of very small phase shifts from spectral interferograms. Because of the excellent shot-to-shot stability of our kilohertz laser system, we are able to average many interferograms *before* phase extraction. This averages and suppresses the noise level, while preserving the stable interference fringes. We are thus able to observe very weak refractive index shifts, with signal levels

smaller than the noise of an interferogram derived from a single shot. The extracted phase $\Delta\Phi$ has an estimated error $(\delta\Phi_{\text{shot}}/N_{\text{int}}^{1/2})(\Delta\Phi)^{-1}$, where $\delta\Phi_{\text{shot}}$ is the maximum phase noise extracted from an individual interferogram, and N_{int} ($=300$) is the number of averaged interferograms.

Figures 6(a) and 6(b) show a beam center lineout and the corresponding $x-t$ perspective plot, respectively, of the alignment recurrences in 7.8 atm D_2 excited by a pump pulse energy of $65 \mu\text{J}$ (peak intensity $4.4 \times 10^{13} \text{ W/cm}^2$). Using $\Delta\alpha_{D_2} = 1.14 \times 10^{-24} \text{ cm}^3$ [49] and $B_{D_2} = 30.4 \text{ cm}^{-1}$ obtained from Fig. 6(c), which will be discussed later, the full revival period is found to be $T = 548 \text{ fs}$, and the molecular alignment calculations using a finite-length pulse and a delta function pulse are shown in Fig. 6(d). In our case, the single-shot temporal window is $\sim 2 \text{ ps}$ long, and we estimate a noise-contributed error of $(\delta\Phi_{\text{shot}}/N_{\text{int}}^{1/2})(\Delta\Phi)^{-1} \sim 2\%$. Earlier measurement of D_2 rotational wave packet using Coulomb explosion imaging [51] showed a revival trace through ~ 0.5 , with error bars comparable to the revival amplitudes.

The calculation of Fig. 6(d) shows that the responses computed with the delta-function pulse and the finite-width pulse are totally different. This is explained by considering the most populous state due to thermal distribution. For D_2 , $j_{\max} \sim 3/4\{1 + [1 + 8/9(k_B T/Bhc)]^{1/2}\} \sim 2-3$,

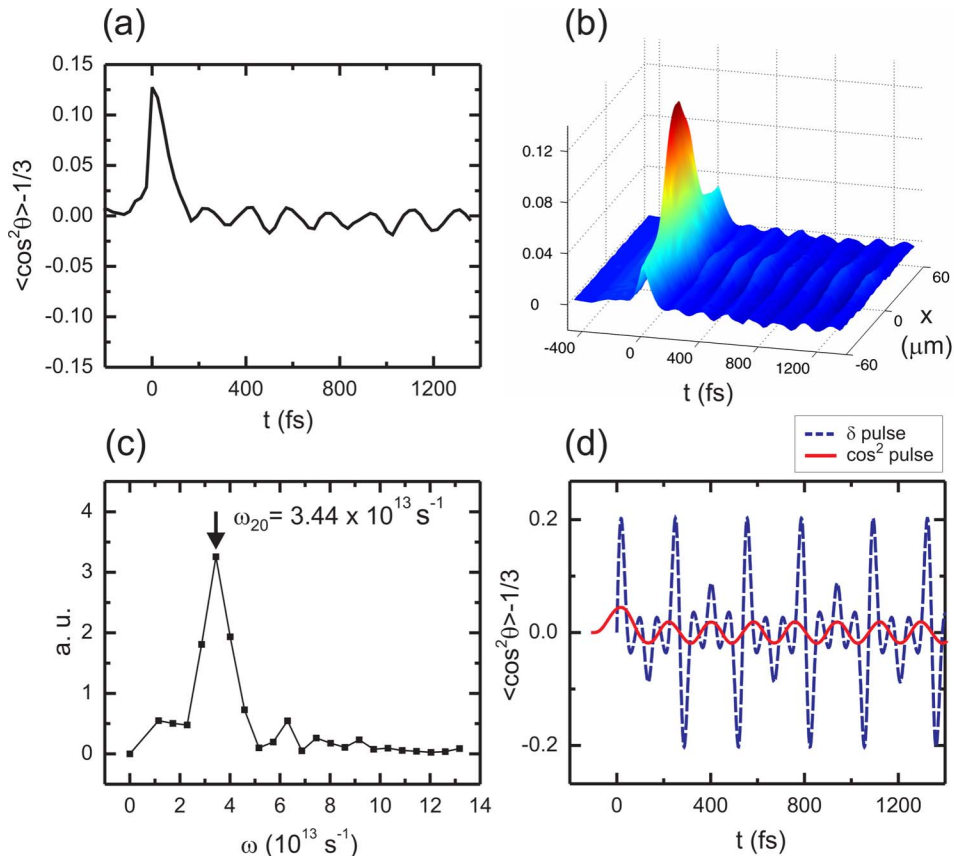


Fig. 6. (Color online) (a) Pump beam center lineout and (b) corresponding $x-t$ perspective plot of measured D_2 molecule alignment recurrences excited by $65 \mu\text{J}$ pump energy ($4.4 \times 10^{13} \text{ W/cm}^2$ peak intensity), with 7.8 atm gas pressure. (c) Fourier transform of the signal representing rotational wave packet revivals after the pump pulse in (a). The peak frequency is identified as $\omega_{2,0} \sim 3.4 \times 10^{13} \text{ s}^{-1}$, giving the rotational constant $B_{D_2} = 30.4 \text{ cm}^{-1}$. (d) Calculated $\langle \cos^2 \theta \rangle_t - 1/3$ with δ function (dashed curve) and 110 fs \cos^2 function (solid curve), using B_{D_2} obtained in (c).

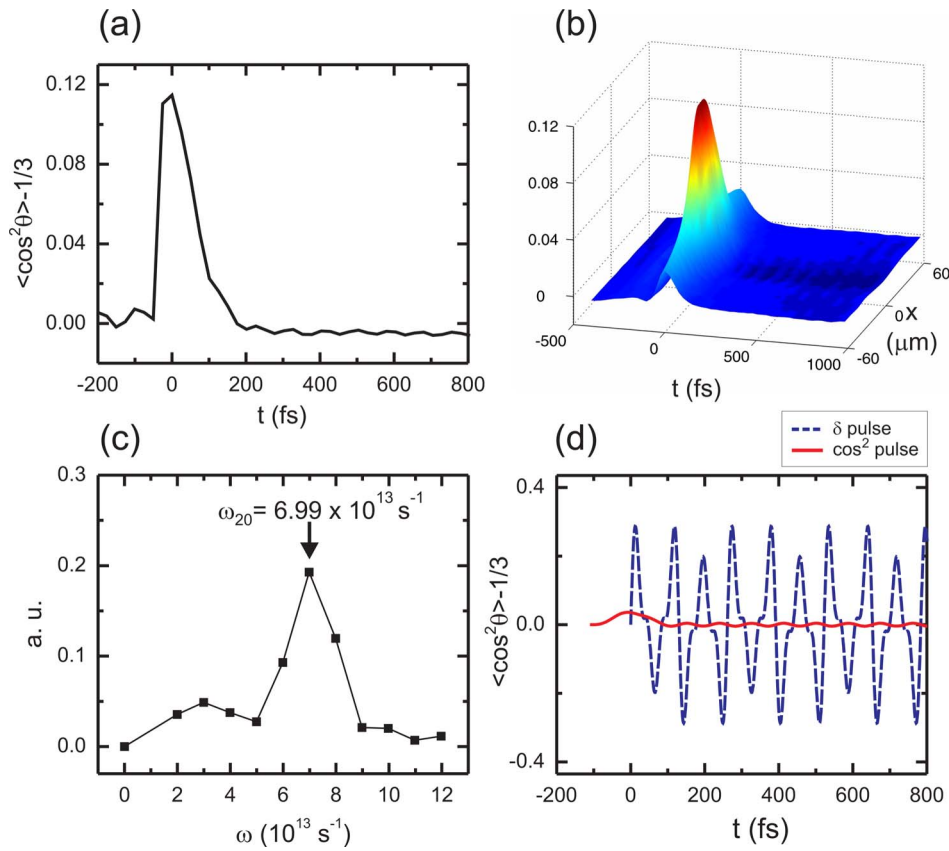


Fig. 7. (Color online) (a) Pump beam center lineout and (b) corresponding $x-t$ perspective plot of H_2 alignment recurrences, measured in the same main conditions as in Fig. 6. (c) $\omega_{2,0} \sim 7 \times 10^{13} \text{ s}^{-1}$ is observed by Fourier transformation of recurrence signal (neglecting the peak) in (a), which gives $B_{\text{H}_2} = 61.8 \text{ cm}^{-1}$. (d) Simulated $\langle \cos^2 \theta \rangle - 1/3$ with δ function (dashed curve) and 110 fs \cos^2 function (solid curve), pump pulses, with rotational constant B_{H_2} from (c).

which is much lower than in O_2 due to its larger B value. We must also take nuclear spin statistics into consideration. For the D_2 molecule, even j states are twice as populated as odd j states because deuterium has nuclear spin $I_N = 1$. Therefore near j_{max} the dominant coupled states with $\Delta j = 2$ required by Eq. (3) are $j = 0, 2$ or $j = 2, 4$, with a frequency spacing $\omega_{2,0} = \omega_2 - \omega_0 \sim 3.4 \times 10^{13} \text{ s}^{-1}$ or $\omega_{4,2} = \omega_4 - \omega_2 \sim 8.0 \times 10^{13} \text{ s}^{-1}$, respectively. Our pump laser bandwidth $\sim 3 \times 10^{13} \text{ s}^{-1}$ can only coherently excite $j = 0$ and 2 states. Figure 6(c) shows the Fourier transform of the temporal response of Fig. 6(a), and the peak frequency can be identified as $\omega_{2,0} = 3.44 \times 10^{13} \text{ s}^{-1}$, giving the rotational constant $B_{D_2} = 30.4 \text{ cm}^{-1}$. This value was used for the calculations of molecular alignment shown in Fig. 6(d), and it agrees well with $B = 29.9 \text{ cm}^{-1}$ from [49].

Results for H_2 are shown in Fig. 7, for the same pressure and pump laser conditions as in the D_2 measurements. The lineout of $\langle \cos^2 \theta \rangle - 1/3$ at the center of pump focal spot is depicted in Fig. 7(a), with its full space-time plot in Fig. 7(b). The effect of wave packet revivals is much weaker than in D_2 . Inspection of Fig. 7(b), showing the small amplitude oscillations following the pump pulse like a transversely localized wake, allows identification of the wiggles in Fig. 7(a) as the real signal from the rotational wave packet. The spectrum of the revival signal in Fig. 7(a) is shown in Fig. 7(c), and again from the peak frequency we get the rotational constant $B_{\text{H}_2} = 61.8 \text{ cm}^{-1}$ and the full revival period $\mathcal{T} = 270 \text{ fs}$, in good agreement

with previous value $B_{\text{H}_2} = 59.3 \text{ cm}^{-1}$ in [49]. As in the case for D_2 , the delta function and finite pulse calculations (employing $\Delta\alpha_{\text{H}_2} = 0.30 \times 10^{-24} \text{ cm}^3$ [49]) show a significant difference because the 110 fs pump pulse bandwidth is too narrow to populate many rotational states. Under our conditions, the most populated state in the excited H_2 wave packet is $j_{\text{max}} \sim 2$. The spin of the hydrogen nucleus

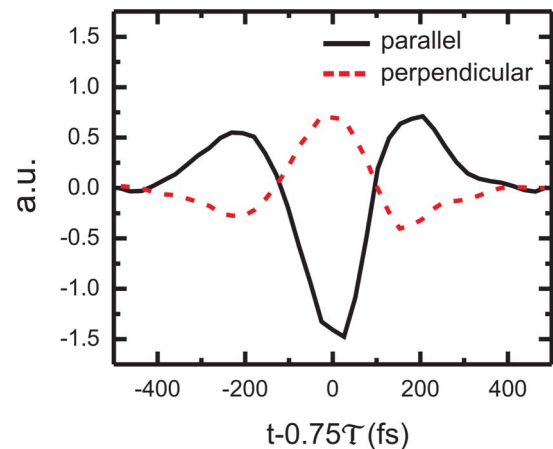


Fig. 8. (Color online) Transient refractive indices of 5.1 atm O_2 near $t = 0.75\mathcal{T}$ for the pump polarization parallel (black solid curve) and perpendicular (red dashed curve) to the probe beam. The pump energy and peak intensity is $40 \mu\text{J}$ and $2.7 \times 10^{13} \text{ W/cm}^2$, respectively.

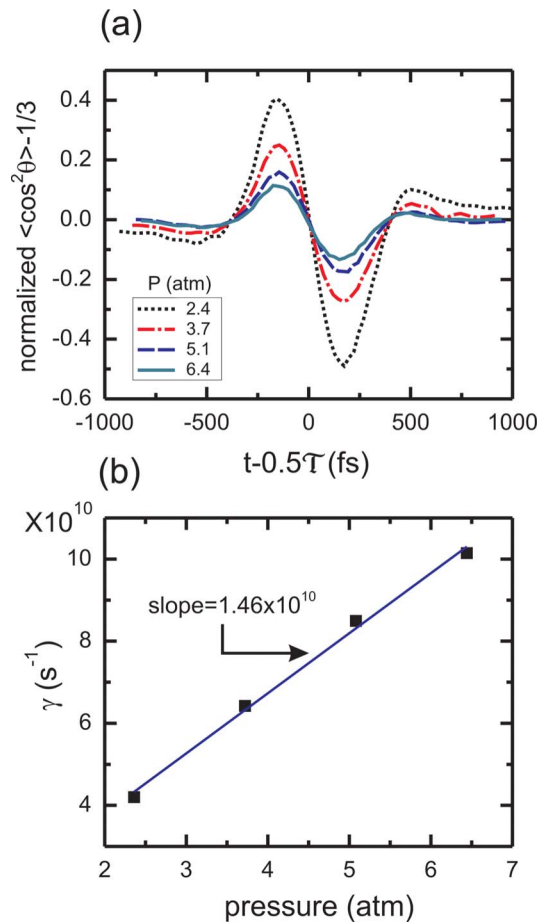


Fig. 9. (Color online) (a) Measured N_2O revivals at $t=0.5T$ at pressures of 2.4, 3.7, 5.1, and 6.4 atm, normalized to the peak alignment amplitude near $t=0$. (b) Dephasing rate γ versus N_2O pressure (squares) with a linear fit (solid line). The dephasing rate per unit pressure is $1.46 \times 10^{10} \text{ s}^{-1} \text{ atm}^{-1}$. The laser energy is $20 \mu\text{J}$, corresponding to $1.4 \times 10^{13} \text{ W/cm}^2$ peak intensity.

is $I_N=1/2$, so that the population of even j states is 3 times greater than odd j states. Therefore the laser pulse likely interacts with the states $j=0,2$, corresponding to $\omega_{2,0} \sim 7 \times 10^{13} \text{ s}^{-1}$, which is more than twice the pump bandwidth. Hence the rotational wavepacket amplitude is expected to be weaker than in the case of D_2 . Also note that for H_2 , the error in the extracted phase shift is estimated to be $(\delta\Phi_{\text{shot}}/N_{\text{int}}^{1/2})(\Delta\Phi)^{-1} \sim 15\%$.

In contrast to the finite pulse simulations [Figs. 6(d) and 7(d)], the experimental results of D_2 and H_2 [Figs. 6(a) and 7(a)] show an initial peak with much higher amplitude than the following revivals. This is because our simulations only compute the rotational effect on the refractive index. Evidently, for D_2 and H_2 (unlike N_2 and N_2O) the contribution of instantaneous nonlinear response n_2I is much larger than the delayed rotational response.

In this paper, we also demonstrate the measurement of molecular alignment at different angles between the pump and probe polarization. The pump polarization is tuned by rotating a HWP in the pump beam path (HWP in Fig. 1). The reflectivity of the dielectric coated beam splitter (BS2 in Fig. 1) is not sensitive to polarization over the range of the pump laser pulse bandwidth. This is veri-

fied by measuring the reflected pump pulse energy while rotating the pump polarization. As an example, for 5.2 atm of O_2 , Fig. 8 compares the response near $t=0.75T$ for pump polarization parallel ($\langle \cos^2 \theta \rangle_t - 1/3$, solid curve) and perpendicular ($1/2 \langle \sin^2 \theta \rangle_t - 1/3$, dashed curve) to the probe. The pump energy and peak intensity are $40 \mu\text{J}$ and $2.7 \times 10^{13} \text{ W/cm}^2$, respectively. As expected, the measured response from perpendicular polarization case has half the magnitude of the parallel polarization case with the sign flipped.

Finally, we present the results of an experiment to observe pressure-dependent wave packet collisional dephasing. Figure 9(a) shows the measured half-revival signals in N_2O normalized to the peak alignment signals near $t=0$, under the same pump laser parameters and varying gas pressure: 2.4, 3.7, 5.1, and 6.4 atm. The dephasing rate γ for each pressure is obtained by fitting exponentials to the amplitudes of a series of successive revivals. The dephasing rate versus N_2O pressure is plotted in Fig. 9(b), which shows a linear dependence as expected from binary collisions. We obtain a dephasing rate per unit pressure $1.46 \times 10^{10} \text{ s}^{-1} \text{ atm}^{-1}$ in N_2O .

7. CONCLUSION

We implemented an improved version of SSSI using a 1 kHz Ti:sapphire regenerative amplifier. By employing a Xe gas cell, only $\sim 300 \mu\text{J}$ is needed to generate energetic, bright, and broadband supercontinuum (SC). The shot-to-shot stability of generated SC pulses is also significantly improved. The instantaneous nonlinear electronic response of monoatomic gas, as well as the delayed rotational response and alignment quantum revivals of linear gas molecules was measured with femtosecond time resolution and micrometer space resolution in a single shot. The collisional dephasing of rotational wave packets was extracted, and a linear relation between dephasing rate and gas pressure was recovered. Finally, the stability of our improved technique makes possible the averaging of interferograms over many shots, allowing extraction of phase shifts smaller than the noise of a single shot. This has enabled, for the first time, the single-shot measurement of rotational wave packet revivals in H_2 and D_2 .

REFERENCES

1. H. Stapelfeldt and T. Seideman, "Aligning molecules with strong laser pulses," *Rev. Mod. Phys.* **75**, 543–557 (2003).
2. R. Velotta, N. Hay, M. B. Mason, M. Castillejo, and J. P. Marangos, "High-order harmonic generation in aligned molecules," *Phys. Rev. Lett.* **87**, 183901 (2001).
3. N. Hay, R. Velotta, M. Lein, R. de Nalda, E. Heesel, M. Castillejo, and J. P. Marangos, "High-order harmonic generation in laser-aligned molecules," *Phys. Rev. A* **65**, 053805 (2002).
4. C. Vozzi, F. Calegari, E. Benedetti, J.-P. Caumes, G. Sansone, S. Stagira, M. Nisoli, R. Torres, E. Heesel, N. Kajumba, J. P. Marangos, C. Altucci, and R. Velotta, "Controlling two-center interference in molecular high harmonic generation," *Phys. Rev. Lett.* **95**, 153902 (2005).
5. J. Itatani, J. Levesque, D. Zeidler, H. Niikura, H. Pepin, J. C. Kieffer, P. B. Corkum, and D. M. Villeneuve, "Tomographic imaging of molecular orbitals," *Nature* **432**, 867–871 (2004).

6. S. Baker, J. S. Robinson, C. A. Haworth, H. Teng, R. A. Smith, C. C. Chirila, M. Lein, J. W. G. Tisch, and J. P. Marangos, "Probing proton dynamics in molecules on an attosecond time scale," *Science* **21**, 424–427 (2006).
7. P. M. Felker, J. S. Baskin, and A. H. Zewail, "Rephasing of collisionless molecular coherence in large molecules," *J. Phys. Chem.* **90**, 724–728 (1986).
8. L. L. Connell, T. C. Corcoran, P. W. Joireman, and P. M. Felker, "Observation and description of a new type of transient in rotational coherence spectroscopy," *J. Phys. Chem.* **94**, 1229–1232 (1990).
9. J. R. Peñano, P. Sprangle, P. Serafim, B. Hafizi, and A. Ting, "Stimulated Raman scattering of intense laser pulses in air," *Phys. Rev. E* **68**, 056502 (2003).
10. E. T. J. Nibbering, G. Grillon, M. A. Franco, B. S. Prade, and A. Mysyrowicz, "Determination of the inertial contribution to the nonlinear refractive index of air, N₂, and O₂ by use of unfocused high-intensity femtosecond laser pulses," *J. Opt. Soc. Am. B* **14**, 650–660 (1997).
11. R. A. Bartels, T. C. Weinacht, N. Wagner, M. Baertschy, Chris H. Greene, M. M. Murnane, and H. C. Kapteyn, "Phase modulation of ultrashort light pulses using molecular rotational wave packets," *Phys. Rev. Lett.* **88**, 013903 (2002).
12. P. W. Dooley, I. V. Litvinyuk, K. F. Lee, D. M. Rayner, M. Spanner, D. M. Villeneuve, and P. B. Corkum, "Direct imaging of rotational wave-packet dynamics of diatomic molecules," *Phys. Rev. A* **68**, 023406 (2003).
13. F. Rosca-Pruna and M. J. J. Vrakking, "Experimental observation of revival structures in picosecond laser-induced alignment of I₂," *Phys. Rev. Lett.* **87**, 153902 (2001).
14. M. A. Duguay and J. W. Hansen, "An ultrafast light gate," *Appl. Phys. Lett.* **15**, 192–194 (1969).
15. E. P. Ippen and C. V. Shank, "Picosecond response of a high-repetition-rate CS₂ optical Kerr gate," *Appl. Phys. Lett.* **26**, 92–93 (1975).
16. J. P. Heritage, T. K. Gustafson, and C. H. Lin, "Observation of coherent transient birefringence in CS₂ vapor," *Phys. Rev. Lett.* **34**, 1299–1302 (1975).
17. R. Righini, "Ultrafast optical Kerr effect in liquids and solids," *Science* **262**, 1386–1390 (1993).
18. V. Renard, O. Faucher, and B. Lavorel, "Measurement of laser-induced alignment of molecules by cross defocusing," *Opt. Lett.* **30**, 70–72 (2005).
19. V. Lorient, E. Hertz, A. Rouzée, B. Sinardet, B. Lavorel, and O. Faucher, "Strong-field molecular ionization: determination of ionization probabilities calibrated with field-free alignment," *Opt. Lett.* **31**, 2897–2899 (2006).
20. J.-F. Ripoche, G. Grillon, B. Prade, M. France, E. Nibbering, R. Lange, and A. Mysyrowicz, "Determination of the time dependence of n_2 in air," *Opt. Commun.* **135**, 310–314 (1997).
21. I. V. Fedotov, A. D. Savvin, A. B. Fedotov, and A. M. Zheltikov, "Controlled rotational Raman echo recurrences and modulation of high-intensity ultrashort laser pulses by molecular rotations in the gas phase," *Opt. Lett.* **32**, 1275–1277 (2007).
22. K. Y. Kim, I. Alexeev, and H. M. Milchberg, "Single-shot supercontinuum spectral interferometry," *Appl. Phys. Lett.* **81**, 4124 (2002).
23. Cl. Froehly, A. Lacourt, and J. Ch. Viénot, "Time impulse response and time frequency response of optical pupils: experimental confirmations and applications," *Nouv. Rev. Opt.* **4**, 183–196 (1973).
24. F. Reynaud, F. Salin, and A. Barthelemy, "Measurement of phase shifts introduced by nonlinear optical phenomena on subpicosecond pulses," *Opt. Lett.* **14**, 275–277 (1989).
25. C. X. Yu, M. Margalit, E. P. Ippen, and H. A. Haus, "Direct measurement of self-phase shift due to fiber nonlinearity," *Opt. Lett.* **23**, 679–681 (1998).
26. J. P. Geindre, P. Audebert, A. Rousse, F. Fallies, J. C. Gauthier, A. Mysyrowicz, A. Dos Santos, G. Hamoniaux, and A. Antonetti, "Frequency-domain interferometer for measuring the phase and amplitude of a femtosecond pulse probing a laser-produced plasma," *Opt. Lett.* **19**, 1997–1999 (1994).
27. P. Salières, L. Le Dèroff, T. Auguste, P. Monot, P. d'Oliveira, D. Campo, J.-F. Hergott, H. Merdji, and B. Carré, "Frequency-domain interferometry in the XUV with high-order harmonics," *Phys. Rev. Lett.* **83**, 5483–5486 (1999).
28. R. Evans, A. D. Badger, F. Fallies, M. Mahdiah, T. A. Hall, P. Audebert, J.-P. Geindre, J.-C. Gauthier, A. Mysyrowicz, G. Grillon, and A. Antonetti, "Time- and space-resolved optical probing of femtosecond-laser-driven shock waves in aluminum," *Phys. Rev. Lett.* **77**, 3359–3362 (1996).
29. J. R. Marquès, J. P. Geindre, F. Amiranoff, P. Audebert, J. C. Gauthier, A. Antonetti, and G. Grillon, "Temporal and spatial measurements of the electron density perturbation produced in the wake of an ultrashort laser pulse," *Phys. Rev. Lett.* **76**, 3566–3569 (1996).
30. C. W. Siders, S. P. Le Blanc, D. Fisher, T. Tajima, M. C. Downer, A. Babine, A. Stepanov, and A. Sergeev, "Laser wakefield excitation and measurement by femtosecond longitudinal interferometry," *Phys. Rev. Lett.* **76**, 3570–3573 (1996).
31. J. R. Marquès, F. Dorchies, F. Amiranoff, P. Audebert, J. C. Gauthier, J. P. Geindre, A. Antonetti, T. M. Antonsen, Jr., P. Chessa, and P. Mora, "Laser wakefield: experimental study of nonlinear radial electron oscillations," *Phys. Plasmas* **5**, 1162–1177 (1998).
32. K. Kim, I. Alexeev, and H. Milchberg, "Single-shot measurement of laser-induced double step ionization of helium," *Opt. Express* **10**, 1563–1572 (2002).
33. S. P. Le Blanc, E. W. Gaul, N. H. Matlis, A. Rundquist, and M. C. Downer, "Single-shot measurement of temporal phase shifts by frequency-domain holography," *Opt. Lett.* **25**, 764–766 (2000).
34. K. Y. Kim, I. Alexeev, E. Parra, and H. M. Milchberg, "Time-resolved explosion of intense-laser-heated clusters," *Phys. Rev. Lett.* **90**, 023401 (2003).
35. I. Alexeev, T. M. Antonsen, K. Y. Kim, and H. M. Milchberg, "Self-focusing of intense laser pulses in a clustered gas," *Phys. Rev. Lett.* **90**, 103402 (2003).
36. K. Y. Kim, I. Alexeev, V. Kumarappan, E. Parra, T. Antonsen, T. Taguchi, A. Gupta, and H. M. Milchberg, "Gases of exploding laser-heated cluster nanoplasmas as a nonlinear optical medium," *Phys. Plasmas* **11**, 2882–2889 (2004).
37. K. Y. Kim, I. Alexeev, and H. M. Milchberg, "Measurement of ultrafast dynamics in the interaction of intense laser pulses with gases, clusters, and plasma waveguides," *Phys. Plasmas* **12**, 056712 (2005).
38. N. H. Matlis, S. Reed, S. S. Bulanov, V. Chvykov, G. Kalintchenko, T. Matsuoka, P. Rousseau, V. Yanovsky, A. Maksimchuk, S. Kalmykov, G. Shvets, and M. C. Downer, "Snapshots of laser wakefields," *Nat. Phys.* **2**, 749–753 (2006).
39. P. B. Corkum, C. Rolland, and T. Srinivasan-Rao, "Supercontinuum generation in gases," *Phys. Rev. Lett.* **57**, 2268–2271 (1986).
40. S. Augst, A. Talebpour, S. L. Chin, Y. Beaudoin, and M. Chaker, "Nonsequential triple ionization of argon atoms in a high-intensity laser field," *Phys. Rev. A* **52**, R917 (1995).
41. S. Geltman, "Multiple ionization of argon atoms by intense laser pulses," *Phys. Rev. A* **54**, 2489–2491 (1996).
42. Y.-H. Chen, S. Varma, I. Alexeev, and H. Milchberg, "Measurement of transient nonlinear refractive index in gases using xenon supercontinuum single-shot spectral interferometry," *Opt. Express* **15**, 7458–7467 (2007).
43. H. J. Lehmeier, W. Leupacher, and A. Renzkofer, "Nonresonant third order hyperpolarizability of rare gases and N₂ determined by third harmonic generation," *Opt. Commun.* **56**, 67–72 (1985).
44. D. Milam and M. J. Weber, "Measurement of nonlinear refractive-index coefficients using time-resolved interferometry: application to optical materials for high-power neodymium lasers," *J. Appl. Phys.* **47**, 2497–2501 (1976).
45. R. Adair, L. L. Chase, and S. A. Payne, "Nonlinear

- refractive-index measurements of glasses using three-wave frequency mixing," *J. Opt. Soc. Am. B* **4**, 875–881 (1987).
46. M. Falconieri, E. Palange, and H. L. Fragnito, "Achievement of $\lambda/4000$ phase distortion sensitivity in the measurement of optical nonlinearities by using a modulated Z-scan technique," *J. Opt. A, Pure Appl. Opt.* **4**, 404–407 (2002).
47. Y.-H. Chen, S. Varma, A. York, and H. M. Milchberg, "Single-shot, space- and time-resolved measurement of rotational wavepacket revivals in H₂, D₂, N₂, O₂, and N₂O," *Opt. Express* **15**, 11341–11357 (2007).
48. W. Demtroder, *Molecular Physics* (Wiley-VCH, 2005).
49. C. H. Lin, J. P. Heritage, T. K. Gustafson, R. Y. Chiao, and J. P. McTague, "Birefringence arising from the reorientation of the polarizability anisotropy of molecules in collisionless gases," *Phys. Rev. A* **13**, 813–829 (1976).
50. I. Alexeev, A. Ting, D. F. Gordon, E. Briscoe, J. R. Penano, R. F. Hubbard, and P. Sprangle, "Longitudinal compression of short laser pulses in air," *Appl. Phys. Lett.* **84**, 4080–4082 (2004).
51. K. F. Lee, F. Legare, D. M. Villeneuve, and P. B. Corkum, "Measured field-free alignment of deuterium by few-cycle pulses," *J. Phys. B* **39**, 4081–4086 (2006).